

Ptychography as a wavefront sensor for high-numerical aperture extreme ultraviolet lithography

Analysis and limitations

Dwivedi, Priya; Pereira, Sylvania F.; Urbach, H. Paul

DOI

[10.1117/1.OE.58.4.043102](https://doi.org/10.1117/1.OE.58.4.043102)

Publication date

2019

Document Version

Final published version

Published in

Optical Engineering

Citation (APA)

Dwivedi, P., Pereira, S. F., & Urbach, H. P. (2019). Ptychography as a wavefront sensor for high-numerical aperture extreme ultraviolet lithography: Analysis and limitations. *Optical Engineering*, 58(4), Article 043102. <https://doi.org/10.1117/1.OE.58.4.043102>

Important note

To cite this publication, please use the final published version (if applicable). Please check the document version above.

Copyright

Other than for strictly personal use, it is not permitted to download, forward or distribute the text or part of it, without the consent of the author(s) and/or copyright holder(s), unless the work is under an open content license such as Creative Commons.

Takedown policy

Please contact us and provide details if you believe this document breaches copyrights. We will remove access to the work immediately and investigate your claim.

Optical Engineering

OpticalEngineering.SPIEDigitalLibrary.org

Ptychography as a wavefront sensor for high-numerical aperture extreme ultraviolet lithography: analysis and limitations

Priya Dwivedi
Silvania F. Pereira
H. Paul Urbach

SPIE.

Priya Dwivedi, Silvania F. Pereira, H. Paul Urbach, "Ptychography as a wavefront sensor for high-numerical aperture extreme ultraviolet lithography: analysis and limitations," *Opt. Eng.* **58**(4), 043102 (2019), doi: 10.1117/1.OE.58.4.043102.

Ptychography as a wavefront sensor for high-numerical aperture extreme ultraviolet lithography: analysis and limitations

Priya Dwivedi,* Sylvania F. Pereira, and H. Paul Urbach

Delft University of Technology, Department of Imaging Physics, Optics Research Group, Faculty of Applied Science, Delft, The Netherlands

Abstract. Wavefront aberration measurements are required to test an extreme ultraviolet (EUV) imaging system. For a high-NA EUV imaging system, where conventional wavefront-sensing techniques show limitations, ptychography can be used for this purpose. However, at the wavelength region of EUV (i.e., 13.5 nm), the position accuracy of the scanning mask that is defined for ptychography is stringent. Therefore, we propose ptychography combined with mask position correction. The simulated intensity patterns, the ones we use, resemble expected EUV experimental data. Finally, we show the results in the presence of Poisson noise and the tolerance of the position correction method for error in mask positions. © The Authors. Published by SPIE under a Creative Commons Attribution 4.0 Unported License. Distribution or reproduction of this work in whole or in part requires full attribution of the original publication, including its DOI. [DOI: [10.1117/1.OE.58.4.043102](https://doi.org/10.1117/1.OE.58.4.043102)]

Keywords: aberrations retrieval; extreme ultraviolet lithography; lensless imaging; phase retrieval; wavefront sensing.

Paper 181689 received Nov. 27, 2018; accepted for publication Mar. 19, 2019; published online Apr. 9, 2019.

1 Introduction

Over the past decades, the semiconductor industry has used optical projection for lithography technology. As the technology advances, the number of transistors on a chip increases exponentially—double every 18 months. Shortening the wavelength of light made this possible. Initially, the wavelength of 436 and 365 nm has been used for chip manufacturing. With these wavelengths, the node size of half a micron has been achieved.¹ To shrink the node size further, deep ultraviolet (248 and 193 nm) wavelengths are used. Afterward, the combination of immersion technology and 193-nm lithography made 45-nm node size possible, and with higher NA, 32 nm of node size can also be achieved. Currently, with the extreme ultraviolet (EUV) wavelength (13.5 nm), 13-nm node size is possible, and at high NA, even smaller features are expected.²

One of the key challenges in EUV lithography (EUVL) is the inspection of the optical system for its aberrations.³ The most widespread method to accurately measure the wavefront and aberrations is interferometry, which is based on the interference pattern created by a reference and a test wave. These interferograms are used for retrieving the wavefront and, eventually, the aberrations in the test wave. At EUV wavelengths, the accuracy for alignment of an optical setup is much more challenging than for optical wavelengths. Therefore, several techniques have been devised that are based on common path interferometry.

For instance, point-diffraction interferometry (PDI) method had been suggested^{4,5} and applied to EUVL.⁶ In this method, a semitransparent membrane with a pinhole, which is placed at the image plane, generate an interference pattern. To create a clear interference pattern, the intensity at the pinhole should be low, which can be achieved by moving the semitransparent membrane from focus to defocus. Consequently, the semitransparent membrane should be

almost opaque to transmit similar intensity of light. This criterion makes the PDI method inefficient for EUVL. Subsequently, phase-shifting point-diffraction interferometer (PS/PDI)^{7,8} was introduced, which was found to be 10 to 100 times more robust than PDI for EUV applications.⁹ Unlike PDI, this method does not require the pinhole to be placed at the low intensity of light. However, this method is limited to imaging systems with low aberrations. Therefore, it is applied to imaging systems which are close to the diffraction-limited quality.

Another successful technique, called shear interferometry, has been devised.¹⁰ It is based on the interference of the test wave with its displaced copy. This technique is more robust than PDI and PS/PDI as it has a higher dynamic range in terms of aberrations. The limitation of this method is that it cannot be used to measure the wavefront accurately near the edge of the pupil. Later on, the Hartmann sensor was introduced to measure the aberrations of the test optics.^{11,12} It is a noninterferometric technique with high efficiency and a lower requirement for the coherence of light. This method uses a grid of small holes in an opaque screen placed in the path of the beam with a CCD camera behind it. Based on the geometrical parameters of the hole size, distance between the mask and the camera, one can reconstruct the wavefront. This method has been applied for EUV application¹³ but not for high-NA EUV.

Lately, one sees a push in the EUV technology toward higher NAs (~0.55). In this case, traditional wavefront sensor techniques fail to address the aberrations, especially when they are large. Therefore, ptychography has been proposed to be used as a wavefront sensor technique.¹⁴ Ptychography is already intensively being used with visible light,^{15,16} x-rays,^{17,18} and e-beams.^{19,20} Now, it is also gaining attention for EUV wavelength.²¹ Ptychography reconstruction depends on the type of the used object and accurately known initial parameters. For short wavelengths, the requirements for accurately known parameters are stringent.

*Address all correspondence to Priya Dwivedi, E-mail: p.dwivedi@tudelft.nl

In this work, we use ptychography to reconstruct the aberrated EUV wavefront with inaccurately known initial parameters, for example, the position of the scanning mask. In Sec. 2, the ptychography and mask position correction algorithm is discussed. The simulation results with mask position errors and with Poisson noise are shown in Sec. 3. Finally, we present possible implications and conclusions in Sec. 4.

2 Ptychography and Position Correction Method

As suggested in the previous section, ptychography iterative engine (PIE)²² is used to reconstruct the aberrated EUV wavefront. In ptychography, an object is scanned by a mask and the corresponding far-field diffraction patterns are captured by the camera. These diffraction patterns are used to reconstruct the object. For short wavelengths, such as x-rays and e-beams, the accuracy of the mask positions should be as high as 50 pm.²³ Hence, to mitigate the requirement for highly accurate mask positions, we use PIE with position correction method.²⁴ The flow chart for the same is shown in Fig. 1.

If the measured intensity pattern for the j 'th mask position is $I^j(\mathbf{u})$, then:

$$I^j(\mathbf{u}) = |\mathcal{F}\{O(\mathbf{r})P(\mathbf{r} - \mathbf{R}^j)\}|^2, \quad (1)$$

where $O(\mathbf{r})$ is the object function, $P(\mathbf{r})$ is the mask function, $\mathbf{R}^j = (X^j, Y^j)$ is the position vector, and \mathcal{F} is the Fourier transform. Here, $j = 1, 2, 3, \dots, J$, where J is the total number of diffraction patterns. If, for k 'th iteration, the estimated object function is $O_k(\mathbf{r})$, with the estimated mask positions $\{\mathbf{R}_k^j\}_{j=1}^J$, the steps for the method are as follows:

Step 1: The exit wave just after the mask is calculated as

$$\psi_k^j(\mathbf{r}) = O_k(\mathbf{r})P(\mathbf{r} - \mathbf{R}_k^j). \quad (2)$$

Step 2: Calculate the far field by taking the Fourier transform of $\psi_k^j(\mathbf{r})$:

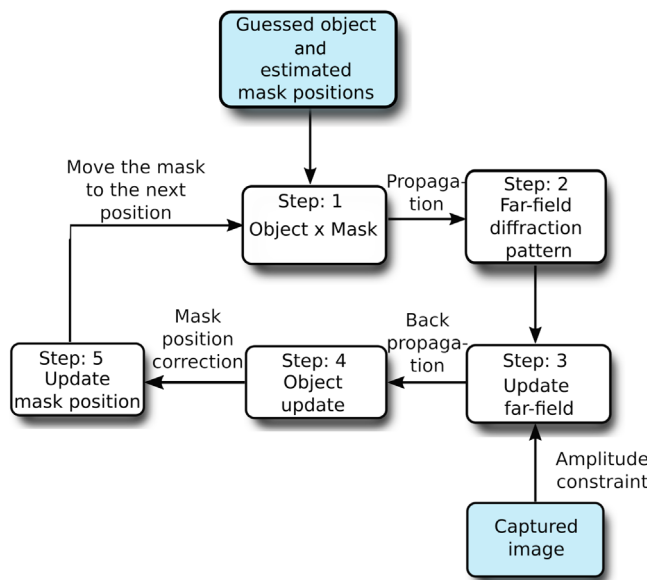


Fig. 1 Flow chart for PIE with mask position correction.

$$\Psi_k^j(\mathbf{u}) = \mathcal{F}\{\psi_k^j(\mathbf{r})\}. \quad (3)$$

Step 3: Apply the amplitude constraint on the estimated far-field as

$$\Psi_k^{ij}(\mathbf{u}) = \sqrt{I^j(\mathbf{u})} \frac{\Psi_k^j(\mathbf{u})}{|\Psi_k^j(\mathbf{u})|}. \quad (4)$$

Step 4: Update the object function using the following equation:

$$O_{k+1}(\mathbf{r}) = O_k(\mathbf{r}) + \frac{P^*(\mathbf{r} - \mathbf{R}_k^j)}{|P^*(\mathbf{r} - \mathbf{R}_k^j)|_{\max}^2} \{\mathcal{F}^{-1}\{\Psi_k^{ij}(\mathbf{u})\} - \psi_k^j(\mathbf{r})\}. \quad (5)$$

Step 5: Update the mask position $\mathbf{R}_k^j = (X_k^j, Y_k^j)$ as

$$X_{k+1}^j = X_k^j - \beta \Delta X_k^j, \quad (6)$$

$$Y_{k+1}^j = Y_k^j - \beta \Delta Y_k^j. \quad (7)$$

Here $\beta = 1$, and

$$\begin{bmatrix} \Delta X_k^j \\ \Delta Y_k^j \end{bmatrix} = (A_k^{jT} A_k^j)^{-1} A_k^{jT} \begin{bmatrix} \Delta I_k^j(1) \\ \Delta I_k^j(2) \\ \vdots \\ \Delta I_k^j(N) \end{bmatrix}, \quad (8)$$

where A_k^j is a $N \times 2$ matrix and A_k^{jT} is its transpose. Here, A_k^j is calculated as

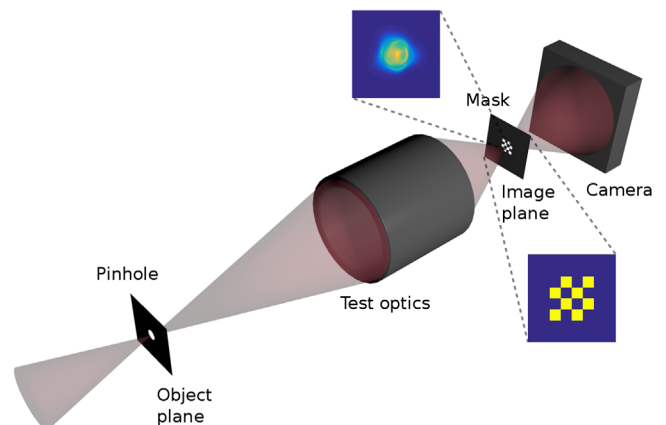


Fig. 2 Setup for reconstructing the wavefront at the image plane and eventually to calculate the present aberrations in the optical system. Illumination is from left.

$$A_k^j = \begin{bmatrix} \frac{\partial I_k^j}{\partial X_k^j}(1) & \frac{\partial I_k^j}{\partial Y_k^j}(1) \\ \frac{\partial I_k^j}{\partial X_k^j}(2) & \frac{\partial I_k^j}{\partial Y_k^j}(2) \\ \vdots & \vdots \\ \frac{\partial I_k^j}{\partial X_k^j}(N) & \frac{\partial I_k^j}{\partial Y_k^j}(N) \end{bmatrix} \quad (9)$$

Step 6: Move the mask to the next position and repeat the steps from 1 to 5.

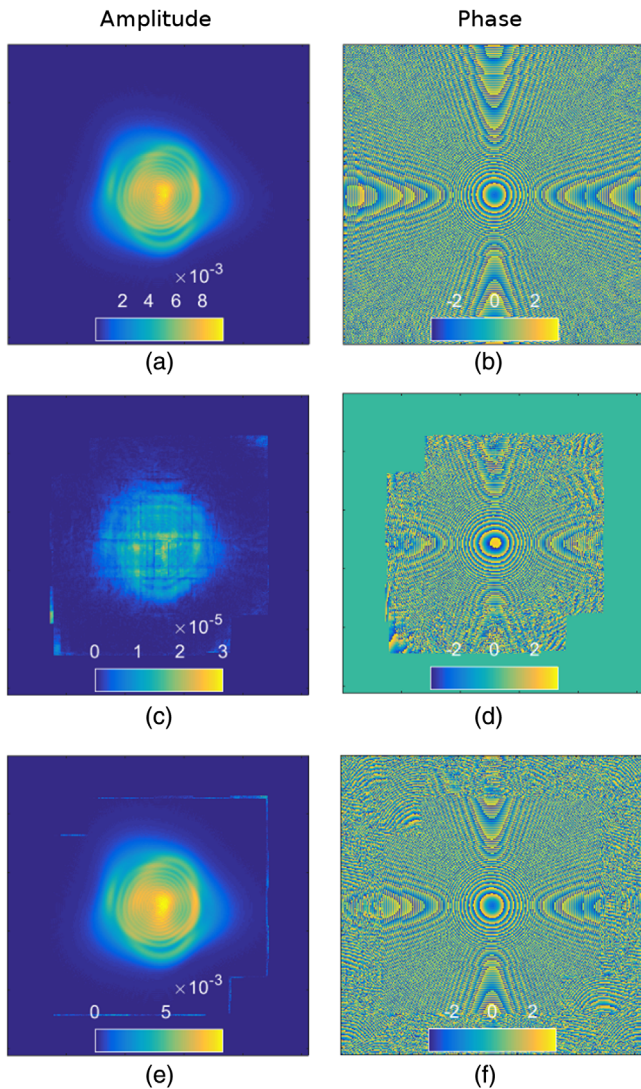


Fig. 3 The reconstructed wavefront amplitude and phase with and without mask position correction. About 7×7 mask positions are used to scan the wavefront where the overlap between the neighboring mask positions is 71.4%. The introduced error in the mask positions varies between $[-5$ and $5]$ pixels ($\sim[-39.05, 39.05]$ nm). (a) and (b) The used wavefront amplitude (varying from 0 to 0.0096) and phase (varying from $-\pi$ to π). (c) and (d) Reconstructed wavefront amplitude and phase without position correction. (e) and (f) Reconstructed wavefront amplitude and phase with position correction.

3 Simulation Results

3.1 Simulations

In Fig. 2, we show the experimental scheme used for calculating the aberrations in the optical system (test optics). The pinhole is placed in the object plane; a checkerboard mask is placed at the image plane. This mask scans the wavefront in the image plane and the corresponding intensity patterns at the far field are recorded in the camera. With ptychography, we reconstruct the wavefront and eventually the present aberrations in the optical system.

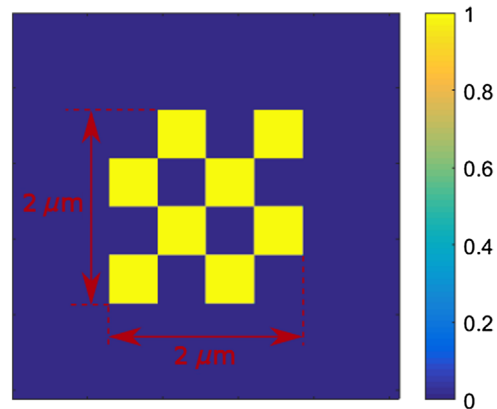


Fig. 4 This mask is used to scan the wavefront and to create the intensity patterns in the far field. The scan is performed in 7×7 rectangular grid with a grid interval of 142.8 nm.

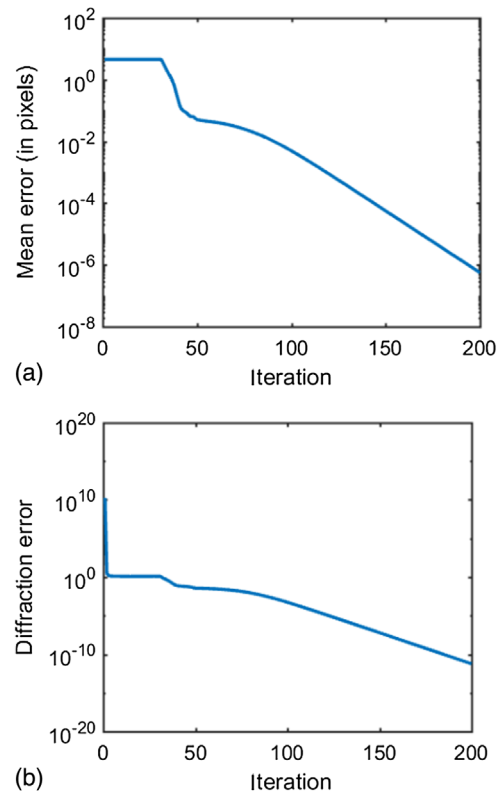


Fig. 5 (a) Mean error in mask positions versus number of iterations. Here, one pixel is equivalent to 7.81 nm. (b) Diffraction error versus number of iterations.

To assess how accurately ptychography with position correction can reconstruct an EUV wavefront, we use the wavefront amplitude and phase as shown in Figs. 3(a) and 3(b). This wavefront amplitude and phase resemble the expected EUV experimental data and the used wavelength of the light is 13.5 nm. It has an approximate size of $2 \mu\text{m} \times 2 \mu\text{m}$ with a field of view of $4 \mu\text{m} \times 4 \mu\text{m}$; here, the wavefront amplitude varies between 0 and 0.0096 and the wavefront phase between $-\pi$ and π . The wavefront is scanned by a $2 \mu\text{m} \times 2 \mu\text{m}$ checkerboard mask, as shown in Fig. 4. The mask is moved on a rectangular grid of 7×7 where the grid interval is 142.8 nm; these mask positions are used for creating the

intensity patterns in the far field. A random initial error taken from $[-5, 5]$ pixels are added to each mask positions; these positions are used as the estimated mask positions. Here, one pixel is equivalent to 7.81 nm.

Figures 3(a) and 3(b) show the wavefront amplitude and phase, which were used to create intensity patterns. Figures 3(c) and 3(d) show the reconstruction when PIE was used, and Figs. 3(e) and 3(f) show the reconstruction when PIE with position correction was used. The mean error of the positions of the mask is shown in Fig. 5(a); it can be clearly seen that the mask positions converge as accurately as 10^{-6} pixels (~ 7.81 fm). Figure 5(b) shows the

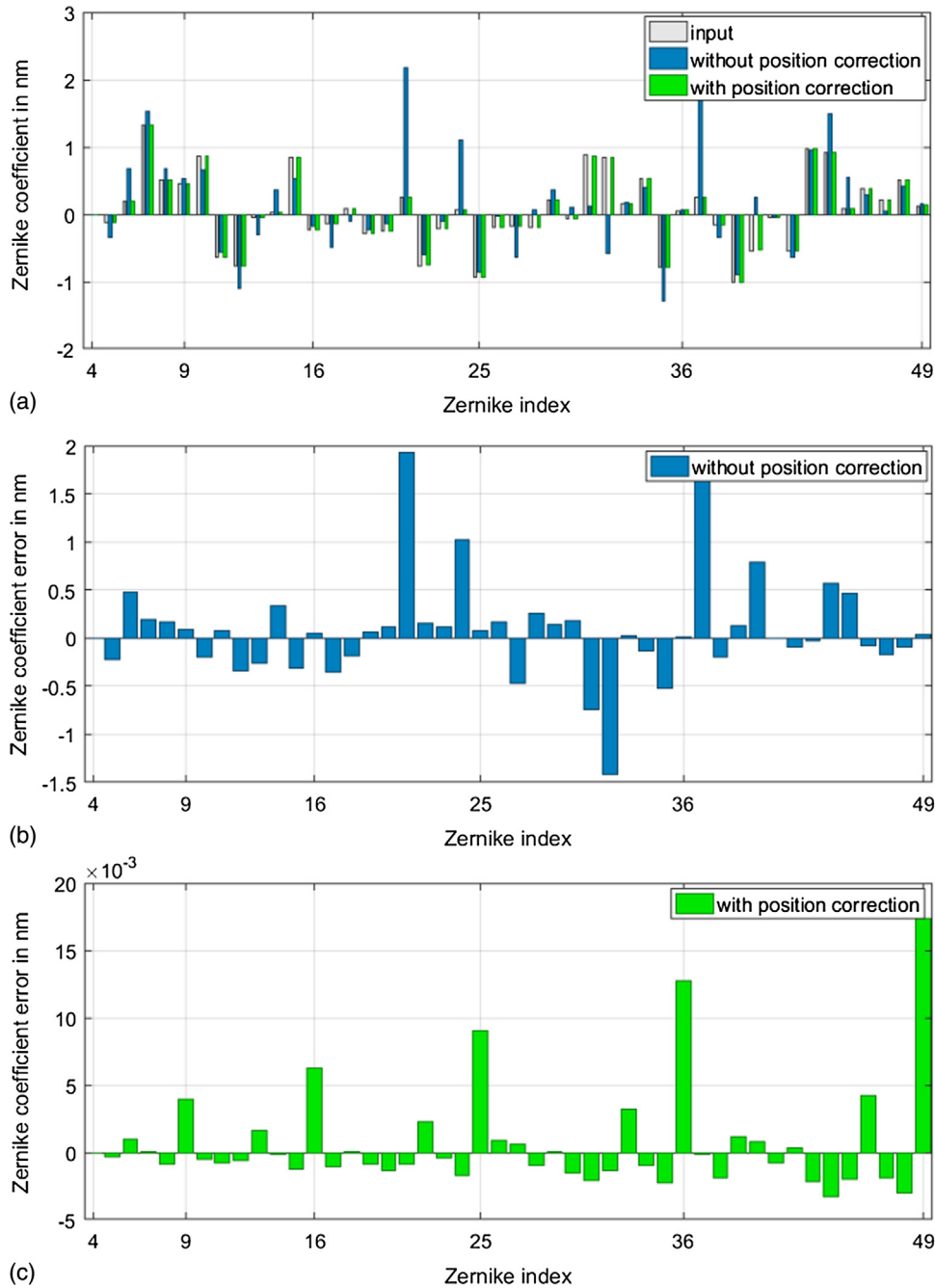


Fig. 6 (a) Zernike coefficient versus Zernike index for the input and for the reconstructed wavefronts. Here, the wavefront is reconstructed with and without position correction. (b) Zernike coefficient error versus Zernike index for the reconstructed wavefront without position correction. (c) Zernike coefficient error versus Zernike index for the reconstructed wavefront with position correction.

diffraction error versus iterations. Here, the diffraction error is the sum of squares error between the measured amplitude and the simulated amplitude in the far field.

The simulated wavefront was generated from an imaging system which had aberrations. These present aberrations are shown in Fig. 6(a) as Zernike plots (gray bars). To see how accurately these aberrations can be reconstructed, in Fig. 6(a), we have shown Zernike coefficient versus Zernike index for the reconstruct wavefront with and without position correction. The errors in the reconstructed Zernike coefficients are also plotted in Figs. 6(b) and 6(c) for the cases when wavefront reconstruction was performed using PIE and PIE with position correction. It can be clearly seen that PIE with position correction has retrieved the Zernike coefficients with an accuracy of 20 pm.

3.2 Effect of Noise in the Presence of Position Errors

As noise is an inevitable part of experimental data, we have performed simulations in the presence of Poisson noise when mask position errors are also present. The simulation parameters are the same as in Sec. 3.1, including the mask position errors. We show the results for the case of 10⁵, 10⁶, 10⁷ number of photons per diffraction pattern. In Fig. 7(a), the diffraction error for varying Poisson noise is plotted. To give an idea of what it means to have an error of 0.45 in diffraction

pattern, we have also shown the measured amplitude, the estimated amplitude, and the difference of the same for one mask position in Fig. 7(b). The corresponding reconstructed wavefront amplitude and phase are shown in Fig. 8. It can be clearly seen that ptychography with position correction can reconstruct the wavefront with 10⁶ photons per diffraction pattern, while also correcting the mask position errors.

3.3 Tolerance for Maximum Mask Positions Error

To find out how much this method can tolerate the error in the mask positions, we performed the simulations for different varying initial error in the mask positions. All other simulation parameters were the same as in Sec. 3.1. Ten simulations were performed for each introduced initial error. In Fig. 9, the solid line represents the mean of the final mask position error for all the 10 simulations, whereas semitransparent patch shows the standard deviation for the same. As can be seen from the plot, the error increases with increasing introduced initial maximum error. When maximum introduced initial error was 5 pixels, i.e., 39 nm, all the simulations converge to the correct solutions. Hence, from these results, one can conclude that the position correction method can tolerate mask position errors as large as 3 times of the wavelength.

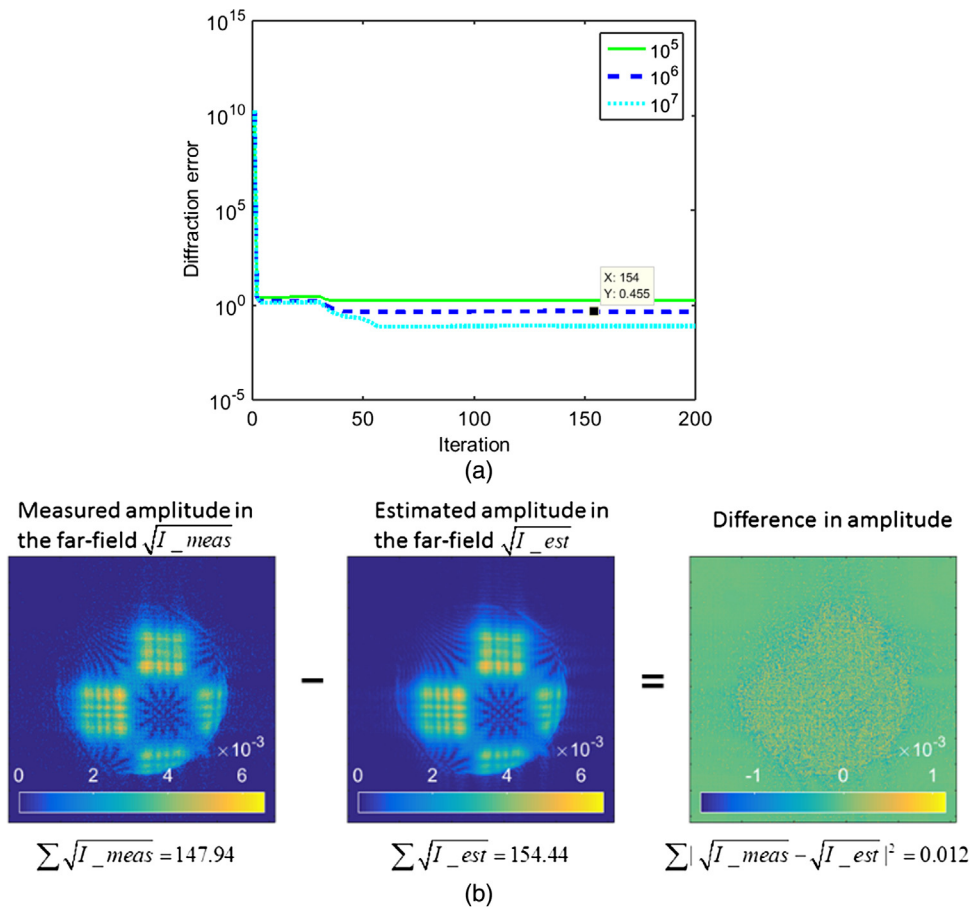


Fig. 7 Reconstruction in the presence of noise. (a) Diffraction error for varying number of photons per diffraction pattern in the presence of mask position error. (b) To show what it means to have an error of 0.45 in diffraction pattern, we have shown the measured amplitude, the estimated amplitude, and the difference between the two for one mask position when the number of photons per diffraction pattern is 10⁶.

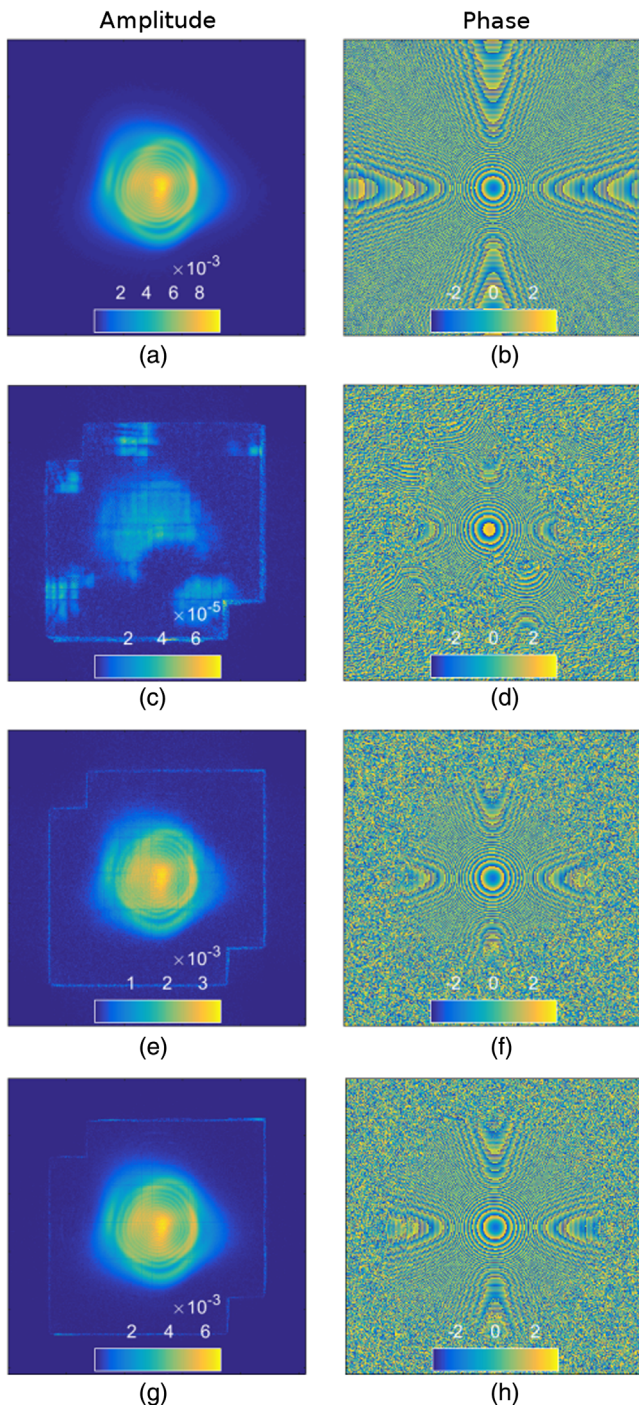


Fig. 8 Reconstructed wavefront with varying number of photons per diffraction pattern in the presence of mask position error; (a) and (b) are the used wavefront amplitude and phase; (c) and (d), (e) and (f), and (g) and (h) are the reconstructed amplitude and phase with 10^5 , 10^6 , and 10^7 number of photons per diffraction pattern, respectively.

4 Discussion and Conclusion

We have implemented ptychography for the application of high-NA EUV wavefront sensor and have shown its robustness and limitations. Ptychography was already suggested for EUV wavefront sensing in Ref. 14. In the present work, we have shown the results with simulated EUV wavefront and have analyzed the reconstructions in the presence of mask position error and Poisson noise.

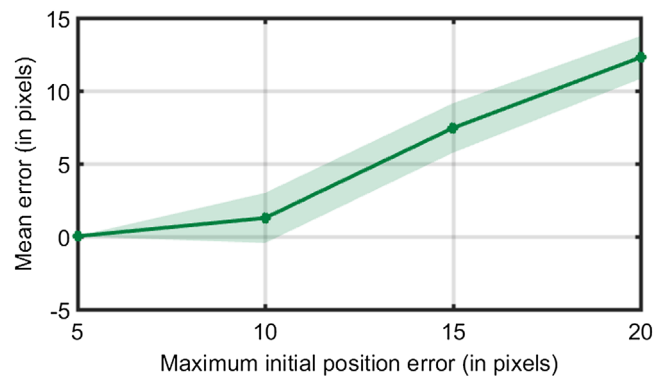


Fig. 9 Mean error versus introduced maximum initial position error. Ten simulations were performed for each introduced maximum initial position error. Solid line represents the mean of the converged error of the 10 simulations, whereas the semitransparent patch shows the standard deviation for the same.

Using simulated data, we have shown that even a mask position error of 39 nm can be corrected with an accuracy of 10^{-6} pixels (~ 7.81 fm). The error in the reconstructed wavefront has been shown in terms of Zernike coefficients. About 20 pm ($\sim 0.0015\lambda$) of error in Zernike coefficient has been achieved for wavefront reconstruction. Furthermore, on performing the simulations in the presence of noise and mask position error, we have found that it can bear Poisson noise of 10^6 number of photons per diffraction pattern in the presence of the mask position error from $[-5$ to $5]$ pixels ($\sim [-39.05, 39.05]$ nm). In addition, we have also shown the results for the tolerance of initial mask position error. These results can stand as a first step for the implementation of ptychography to EUV wavefront sensing applications.

Acknowledgments

The research has received funding from the people program (Marie Curie Actions) of the European Union's Seventh Framework Programme (FP72007-2013) under REA Grant Agreement No. PITN-GA-2013-608082.

References

1. B. Wu and A. Kumar, "Extreme ultraviolet lithography: a review," *J. Vac. Sci. Technol. B* **25**, 1743 (2007).
2. V. Bakshi, *EUV Lithography*, 2nd ed., SPIE Press, Bellingham, Washington (2018).
3. V. Bakshi, *EUV Lithography*, SPIE Press, Bellingham, Washington (2009).
4. W. P. Linnik, "A simple interferometer for the investigation of optical systems," *Proc. Acad. Sci. USSR* **1**, 208 (1933).
5. R. N. Smartt and W. H. Steel, "Theory and application of point-diffraction interferometers (telescope testing)," *Jpn. J. Appl. Phys.* **14**, 351–356 (1975).
6. K. A. Goldberg et al., "At-wavelength testing of optics for EUV," *Proc. SPIE* **2437**, 347–354 (1995).
7. H. Medeck et al., "Phase-shifting point diffraction interferometer," *Opt. Lett.* **21**(19), 1526–1528 (1996).
8. E. Tejnjl et al., "At-wavelength interferometry for extreme ultraviolet lithography," *J. Vac. Sci. Technol.* **15**(9), 2455 (1997).
9. K. A. Goldberg, "Extreme ultraviolet interferometry," PhD Thesis, University of California, Berkeley (1997).
10. H. H. Hopkins, "Interferometric methods for the study of diffraction images," *Opt. Acta Int. J. Opt.* **2**(1), 23–29 (1955).
11. I. Ghozeil, *Optical Shop Testing*, Wiley, New York (1992).
12. A. Polo et al., "Determination of wavefront structure for a Hartmann wavefront sensor using a phase-retrieval method," *Opt. Express* **20**, 7822–7832 (2012).
13. P. Mercere et al., "Hartmann wave-front measurement at 13.4 nm with $\frac{\lambda}{120}$ accuracy," *Opt. Lett.* **28**(17), 1534–1536 (2003).

14. A. Wojdyla, R. Miyakawa, and P. Naulleau, "Ptychographic wavefront sensor for high-NA EUV inspection and exposure tools," *Proc. SPIE* **9048**, 904839 (2014).
15. J. M. Rodenburg, A. C. Hurst, and A. G. Cullis, "Transmission microscopy without lenses for objects of unlimited size," *Ultramicroscopy* **107**(2–3), 227–231 (2007).
16. A. M. Maiden, J. M. Rodenburg, and M. J. Humphry, "Optical ptychography: a practical implementation with useful resolution," *Opt. Lett.* **35**(15), 2585–2587 (2010).
17. J. M. Rodenburg et al., "Hard-x-ray lensless imaging of extended objects," *Phys. Rev. Lett.* **98**(3), 034801 (2007).
18. P. Thibault et al., "High-resolution scanning x-ray diffraction microscopy," *Science* **321**(5887), 379–382 (2008).
19. F. He et al., "Wave-front phase retrieval in transmission electron microscopy via ptychography," *Phys. Rev. B: Condens. Matter* **82**(12), 121415 (R) (2010).
20. J. M. Humphry et al., "Ptychographic electron microscopy using high-angle dark-field scattering for sub-nanometre resolution imaging," *Nat. Commun.* **3**, 730 (2012).
21. P. Helfenstern et al., "Coherent diffractive imaging methods for semiconductor manufacturing," *Adv. Opt. Technol.* **6**(6), 439–448 (2017).
22. H. M. L. Faulkner and J. M. Rodenburg, "Movable aperture lensless transmission microscopy: a novel phase retrieval algorithm," *Phys. Rev. Lett.* **93**(2), 023903 (2004).
23. F. Zhang et al., "Translation position determination in ptychographic coherent diffraction imaging," *Opt. Express* **21**, 13592–13606 (2013).
24. P. Dwivedi et al., "Lateral position correction in ptychography using the gradient of intensity patterns," *Ultramicroscopy* **192**, 29–36 (2018).

Priya Dwivedi received her master's degree in applied physics from Indian Institute of Technology (Indian School of Mines), Dhanbad, in 2013. She started her PhD in the optics group, Faculty of Applied Sciences, Delft University of Technology, The Netherlands, in 2014. Her research interests mainly focus on phase retrieval techniques.

Silvania F. Pereira is an associate professor of applied sciences at Delft University of Technology, The Netherlands. Her research interests include Fourier scatterometry, optimization of the electric field in focus, extended Nijboer–Zernike (ENZ) theory, novel storage methods for optical disk systems. She is the (co-)author of several scientific papers, two U.S. patent and has participated in the European projects MoreMoore, SLAM, SPAM, SURPASS, Clean4Yield, and the European Network in Micro-optics NEMO.

H. Paul Urbach has been a full professor and head of the optics research group at Delft University of Technology, The Netherlands, since January 2008. He received his PhD from the University of Groningen, The Netherlands, in 1986. His research interests include many branches of optics, such as optical lithography for ICs and optical disk mastering, x-ray fluorescence, electromagnetic modeling of optical recording, manipulation of spontaneous emission, high-numerical aperture imaging, photoactive anisotropic media, and plasmonics for application in light-emitting diodes.